



## NRC Publications Archive Archives des publications du CNRC

### **An experimental and numerical study of particle size distribution effects on the sintering of porous ceramics**

Darcovich, Kenneth; Toll, Floyd; Hontanx, Pierre; Roux, Virginie; Shinagawa, Kazunari

This publication could be one of several versions: author's original, accepted manuscript or the publisher's version. / La version de cette publication peut être l'une des suivantes : la version prépublication de l'auteur, la version acceptée du manuscrit ou la version de l'éditeur.

For the publisher's version, please access the DOI link below. / Pour consulter la version de l'éditeur, utilisez le lien DOI ci-dessous.

#### **Publisher's version / Version de l'éditeur:**

[https://doi.org/10.1016/S0921-5093\(02\)00634-2](https://doi.org/10.1016/S0921-5093(02)00634-2)

*Materials Science and Engineering A*, 348, May, pp. 76-83, 2003

#### **NRC Publications Record / Notice d'Archives des publications de CNRC:**

<https://nrc-publications.canada.ca/eng/view/object/?id=54f24dde-4a9b-4fb5-bf63-cb6a4a7033f7>

<https://publications-cnrc.canada.ca/fra/voir/objet/?id=54f24dde-4a9b-4fb5-bf63-cb6a4a7033f7>

Access and use of this website and the material on it are subject to the Terms and Conditions set forth at

<https://nrc-publications.canada.ca/eng/copyright>

READ THESE TERMS AND CONDITIONS CAREFULLY BEFORE USING THIS WEBSITE.

L'accès à ce site Web et l'utilisation de son contenu sont assujettis aux conditions présentées dans le site

<https://publications-cnrc.canada.ca/fra/droits>

LISEZ CES CONDITIONS ATTENTIVEMENT AVANT D'UTILISER CE SITE WEB.

**Questions?** Contact the NRC Publications Archive team at

PublicationsArchive-ArchivesPublications@nrc-cnrc.gc.ca. If you wish to email the authors directly, please see the first page of the publication for their contact information.

**Vous avez des questions?** Nous pouvons vous aider. Pour communiquer directement avec un auteur, consultez la première page de la revue dans laquelle son article a été publié afin de trouver ses coordonnées. Si vous n'arrivez pas à les repérer, communiquez avec nous à PublicationsArchive-ArchivesPublications@nrc-cnrc.gc.ca.



# An experimental and numerical study of particle size distribution effects on the sintering of porous ceramics<sup>☆</sup>

Ken Darcovich<sup>a,\*</sup>, Floyd Toll<sup>a</sup>, Pierre Hontanx<sup>b</sup>, Virginie Roux<sup>c</sup>,  
Kazunari Shinagawa<sup>d</sup>

<sup>a</sup> Institute for Chemical Process and Environmental Technology, National Research Council of Canada, Ottawa, Ont., Canada K1A 0R6

<sup>b</sup> ICAM-Toulouse, 75, av. de Grande Bretagne, 31300 Toulouse, France

<sup>c</sup> ICAM-Nantes, 35, av. du Champ des Manoeuvres, 44470 Carquefou, France

<sup>d</sup> Department of Advanced Materials Science, Faculty of Engineering, Kagawa University, Hayashi-cho 2217-20, Takamatsu 761-0396, Japan

Received 7 December 2001; received in revised form 28 August 2002; accepted 9 September 2002

## Abstract

A single-step processing method has been established to prepare asymmetric porous alumina microstructures by a controlled sedimentation technique. Fine powder from an aqueous suspension is consolidated over a casting slab. Metastable surface chemical control of the suspension properties was able to induce a highly porous flat disc structure with a continuously increasing mean pore size from top to bottom. Formation of this gradient structure was facilitated by using a powder with a very broad particle size distribution. These structures can be used as either ultrafiltration media or as substrates for inorganic membrane making. Sintering can readily introduce defects into functionally gradient ceramics. Despite these problems, the asymmetric structures considered in this paper can be readily sintered without warpage or cracking. In this regard, a finite element method numerical simulation had been developed to model the sintering characteristics of functionally gradient ceramic structures. The key for being able to predict a non-warped structure was the incorporation into the model of the powder particle size distribution as a field variable. Across the vertical section of the structure, the distributions were broad and overlapping, all with a significant fines tail. These characteristics accelerate and homogenize local sintering rates, such that the net result is a non-warped fused structure. This paper presents recent advances with the simulation, where sample geometry, porosity and particle size distribution evolutions were traced alongside measurements made on physical specimens. In general the model corresponded well with the experimental observations. The correct accounting of observed trends lends confidence to the underlying sintering mechanisms incorporated into the model.

© 2002 Elsevier Science B.V. All rights reserved.

**Keywords:** Numerical study; Particle size distribution; Porous ceramics; Sintering

## 1. Introduction

As part of an on-going project, porous structures expressly intended as membrane substrates have been prepared via a polydisperse slurry sedimentation method which yields a functionally gradient material. The benefit of creating an asymmetric microstructure is to produce a smaller substrate pore size over a thinner

region, thereby imparting superior permeation properties.

Preliminary work has demonstrated the viability of this method for preparing functionally gradient samples made from  $\alpha$ -alumina which retain a high porosity after sintering [1]. Hardness testing was used to demonstrate that the bodies fused and strengthened without significant densification, and hardness gradients measured across the cross-section reflected a functionally gradient microstructure [2]. The dispersion of a small amount of fines throughout the body, promoted through the metastable nature of the suspensions, served as localized sites from which sintering was enabled at lower temperatures, sufficient to fuse the sample into a contiguous hardened porous structure. SEM images demonstrated

<sup>☆</sup> NRCC No. 44390.

\* Corresponding author. Tel.: +1-613-993-6848; fax: +1-613-941-2529

E-mail address: ken.darcovich@nrc.ca (K. Darcovich).

the continuously increasing mean particle size across the cross-section of the samples [3]. Porosimetric measurements on horizontal sections of the samples corroborated the previous findings [1].

It has been shown that the colloidal state or suspension microstructure can be controlled with pH and polyelectrolyte stabilizing additives. Relevant stability criteria for systems such as presently under consideration here are available in the literature [4]. The colloidal phase state of a suspension which forms the consolidated green body has a direct bearing on the eventual microstructure of the sintered solid object [5,6]. By controlling the dispersity of a suspension, slight aggregation and/or hierarchical clusters can contribute to overall porosity increases while at the same time producing a relatively fine pored top surface. Warping and cracking problems were resolved by controlling the particle zeta potential in the suspension so that very fine particles were associated with all size classes, and were present in all vertical positions of the consolidated structure [2].

The sintering of functionally gradient materials has also been a topic of recent interest. Numerical simulations of sintering have been developed to assess mechanistic theories of sintering based on powder compact properties [7,8]. It was known from experiments that local distribution effects can override tendencies that would otherwise be predicted considering only mean powder properties. Our previous paper presented a model formulation to explicitly account for particle size distribution effects [9].

In continuing this thread, it is therefore the main objective of this paper to detail a verification of our simulation output against experimental measurements taken from functionally gradient ceramic structures in both the green and sintered states.

## 2. Constitutive model for sintering

A constitutive model for sintering ceramic powders originally developed by Shinagawa and Hirashima [10] is outlined briefly below. Full details of the formulation are given elsewhere [9].

The principal components of the sintering model are as follows.

An expression from Coble [11] was employed as the basis for sintering deformation under grain boundary diffusion:

$$\dot{\epsilon} = \frac{47\Omega h D_b \sigma}{kT d^3} = \frac{\sigma}{3\eta} \quad (1)$$

where  $\Omega$  is the atomic volume,  $h$  is the width of the grain boundary,  $D_b$  is the grain boundary diffusion coefficient,  $k$  is Boltzmann's constant,  $T$  is the absolute

temperature and  $d$  is the grain size. From Eq. (1), a number of the parameters can be lumped to give  $\eta$ , the sintering viscosity, which can be considered as a measure of a material's resistance to sintering.

As given by Shinagawa, [7] the constitutive equation for the strain rate  $\dot{\epsilon}_{ij}$ , is,

$$\dot{\epsilon}_{ij} = \frac{1}{2\eta} \frac{1}{\rho^{2n-1}} \left\{ \sigma'_{ij} + \delta_{ij} \frac{2}{9f^2} (\sigma_m + \sigma_s) \right\} \quad (2)$$

Above,  $\rho$  is the relative density,  $\sigma'$  is the deviatoric stress,  $\sigma_m$  is the hydrostatic stress,  $\sigma_s$  is the sintering stress, and  $f$  and  $n$  are empirical parameters.

This strain rate is related to the induced sintering stress, [8]

$$\sigma_s = \rho^N \frac{2\gamma}{\zeta R} \left\{ \frac{\rho}{\rho_0} \frac{(1 - \rho_0)^{1/3}}{(1 - \rho)} \right\} \quad (3)$$

where  $\gamma$  is the solid surface tension,  $R$  is the particle radius,  $\rho_0$  is the initial relative density, and  $\zeta$  and  $N$  are constants.

The flow stress of powder particles during sintering can be expressed from Eqs. (1)–(3), leading to the stress–strain rate relations,

$$\{\sigma\} = [D]\{\dot{\epsilon}\} = [D][B]\{u\} \quad (4)$$

where  $[B]$  is the strain rate matrix, elements of  $[D]$  are strain coefficients and  $\{u\}$  is the nodal velocity vector. Eq. (4) can be discretized for the finite element method.

The local influence of powder distributions was incorporated into the model with the relation [12]:

$$\frac{\partial \mathcal{F}}{\partial t} + \frac{\partial}{\partial r} \left( \frac{C_G \mathcal{F}}{r^n} \left( \frac{1}{r_c} - \frac{1}{r} \right) \right) = 0 \quad (5)$$

Eq. (5) enables each radius  $r$  and its corresponding frequency  $\mathcal{F}$  to be solved together in a marching algorithm tracking local particle size distribution evolution. The parameter  $C_G$  is described by Greenwood [13]. It can be expanded as:

$$C_G = \frac{2D_b S \gamma \Omega}{kT} \quad (6)$$

Above,  $S$  is the solubility of a particle of infinite radius, referring to the solid–gas sintering system and  $D_b$  is the grain boundary diffusion coefficient. For alumina at 1500 °C,  $C_G$  was estimated as 0.02283  $\mu\text{m}^3 \text{min}^{-1}$  for the grain boundary diffusion case [9].

To account for all pair interactions throughout the entire particle size distribution, the parameter  $\eta$  from Eq. (1) is adjusted according to:

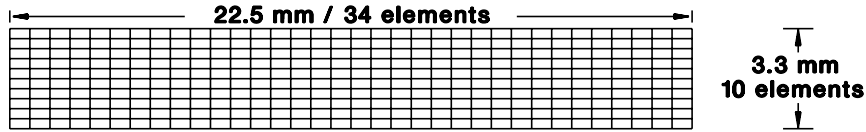


Fig. 1. FEM grid used for numerical simulations.

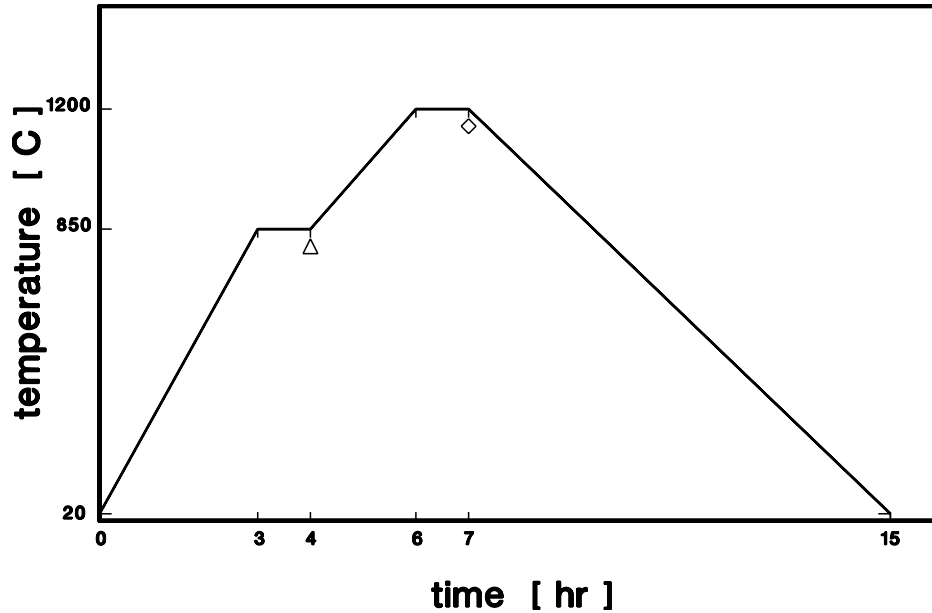


Fig. 2. Ramp and soak sintering profile.

$$\eta_{\text{PSD}} = \left( \frac{\int_{r_s}^{r_b} \int_{r_s}^{r_b} \eta(r_i, r_b) \mathcal{F}(r_i) \mathcal{F}(r_b) dr_i dr}{\int_{r_s}^{r_b} \int_{r_s}^{r_b} \mathcal{F}(r_i) \mathcal{F}(r_b) dr_i dr} \right) \left( \frac{C_{N_{\text{AVG}}}}{C_{N_{\text{PSD}}}} \right) \quad (7)$$

Above  $C_N$  refers to the coordination number of the powder pack. The particle pair interaction term:

$$\eta(r_i, r_b) = 8K_E \frac{r_i^{3.4725}}{r_b^{0.4725}} \quad (8)$$

comes from a derivation by Pan et al. [14] where  $K_E$  is a parameter deduced from the Coble equation, equal to  $kT/47\Omega hD_b\sigma$ .

In order to allow the particle size distribution effects to manifest themselves in a two-dimensional fashion, it was necessary to introduce a temperature field over the sample domain in the simulation. The structure was modeled in two dimensions on an 11 by 35 grid shown in Fig. 1. For a rectangular slab, heating by conduction was considered. The well known conduction equation, given below was employed.

$$\frac{\partial^2 T}{\partial x^2} + \frac{\partial^2 T}{\partial y^2} = \frac{\rho c}{k_T} \frac{\partial T}{\partial t} \quad (9)$$

Above,  $x$  and  $y$  refer to horizontal and vertical coordinates, respectively,  $c$  is the heat capacity and  $k_T$  is the thermal conductivity. Data from the literature was found for alumina for  $c$  and  $k_T$  across the relevant temperature range [15,16].

As a boundary condition, the outside surface temperature of the structure was considered to be equal to the temperature according to the sintering time–temperature profile. As an initial condition, the entire structure was considered to be at 20 °C at the start of the sintering program. The time–temperature sintering profile used for these simulations and in the experiments is given in Fig. 2.

### 3. Experimental

The Ceralox APA-0.2 alumina powder was chosen for this work. It had a broad particle size distribution, and was known to produce consolidated ceramic pieces with a functionally gradient structure. The APA-0.2 powder had a specific surface area of 40.0 m<sup>2</sup> g<sup>-1</sup>, a high value since it has a substantial tail of fines in the distribution, and it occurs in the form of aggregates of ultra-fine particles. The data for specific surface area were taken from product technical information provided by the suppliers. Powder size distributions were determined



Fig. 3. Sectioning method to obtain vertical resolution for local sample microstructure data.

using a Horiba model LA-920 Particle Size Analyzer, which is a laser diffraction device.

Full details on the sample preparation and characterization are given in a previous paper [1]. A brief outline of procedures is given below. Aqueous alumina suspensions were prepared at solids loadings of 5 volume percent solids (v/o), and a steric effect was provided by the addition of an ammonium polymethylacrylic acid electrolyte at a level of  $0.5 \text{ g m}^{-2}$  ( $\text{NH}_4^+ \text{PMA}^-$ ) of molecular weight of approximately 15000 (Darvan C, R.T. Vanderbilt Co. Inc., Norwalk, CT).

The ceramic structures were then produced by sedimentation of the slurries in 45 mm diameter tube sections over milled gypsum slabs, such that they consolidate to form flat discs 3.3 mm thick. Prior to

sintering, the green bodies were dried in an oven at  $50^\circ\text{C}$ . The sintering ramp and soak profiles followed in the experiments are shown in Fig. 2.

Pore size distributions of the sintered ceramic structures were obtained with a Quantachrome Pore Master 60 mercury porosimeter.

### 3.1. Sample series

In order to compare the evolution of samples undergoing sintering with the progress predicted by the numerical simulation, a number of different samples were prepared for analysis. In reference to the ramp and soak profile, (Fig. 2), samples were obtained as follows:

- three samples of the green body (non-sintered);
- samples at  $850^\circ$  ( $\Delta$  on Fig. 2);
- samples at  $1200^\circ$  ( $\diamond$  on Fig. 2).

To obtain these samples, the sintering oven was briefly opened and the discs were removed in the middle of the heat treatment program.

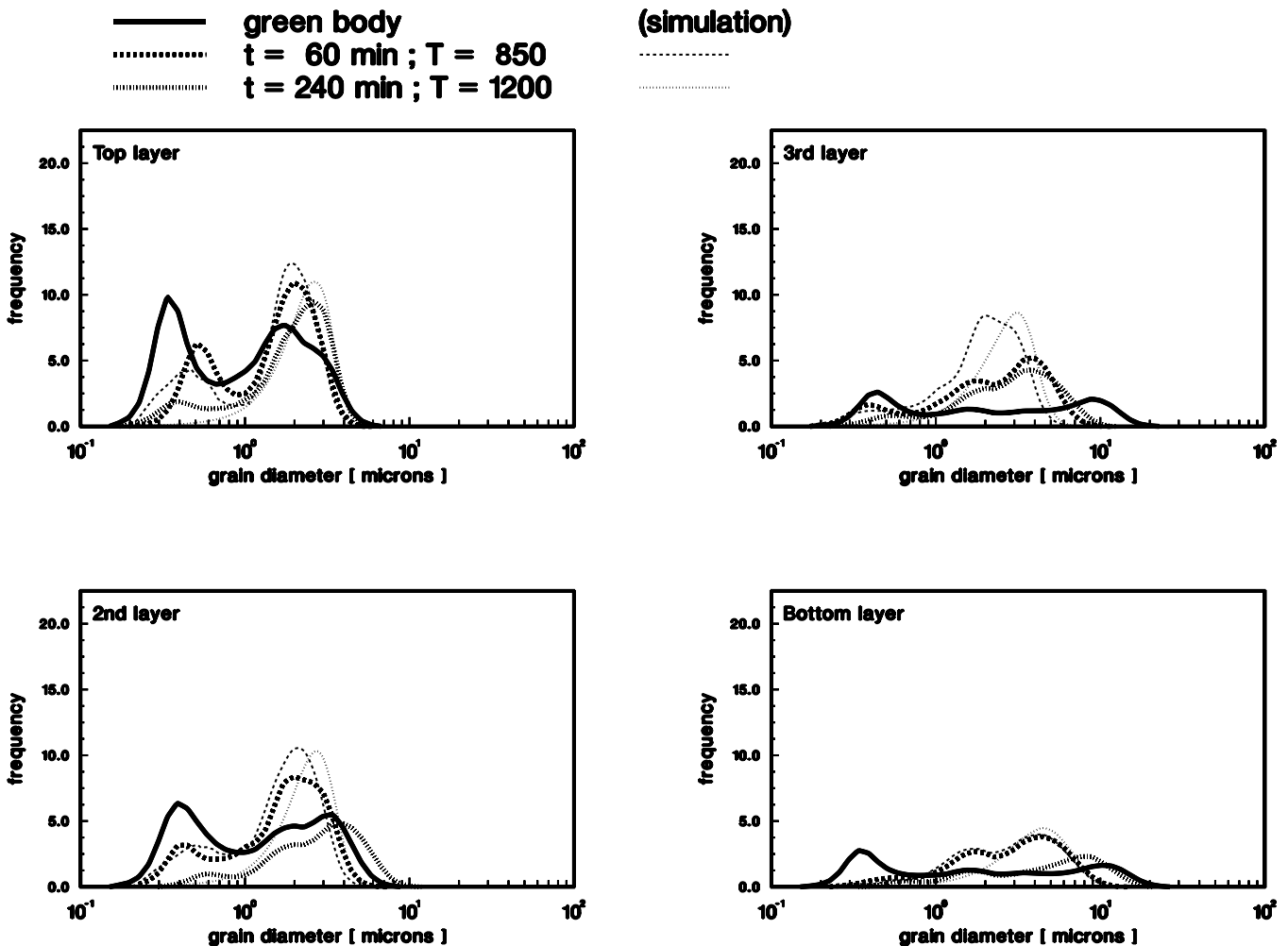
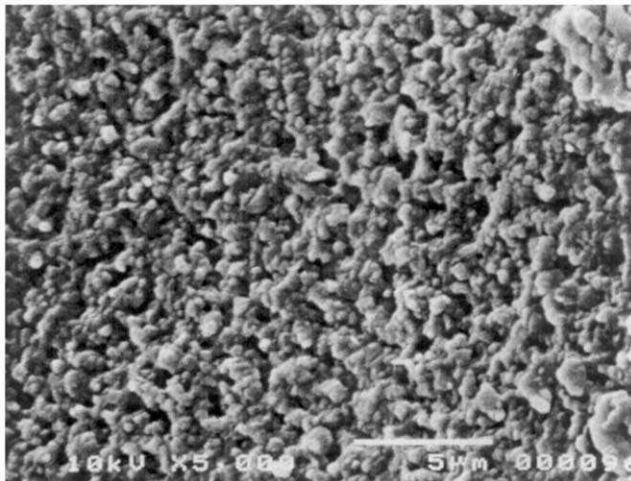
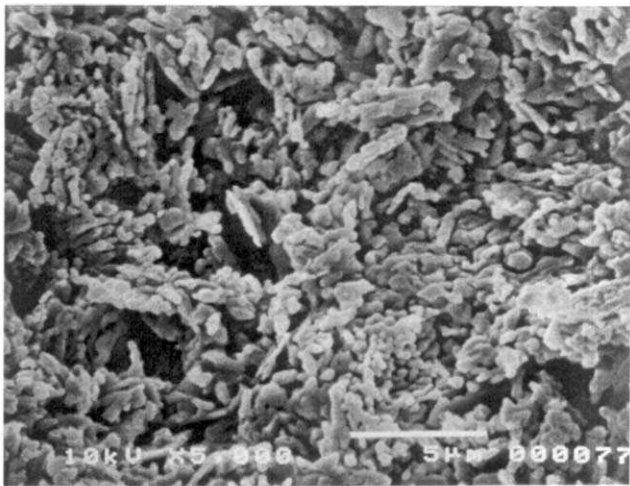


Fig. 4. Particle size distribution evolution from both the numerical simulation and the experimental data.



(a) Top layer



(b) Third layer

Fig. 5. SEM images of the vertical faces of fracture planes from the samples sintered at 1200 °C. (a) Top layer (b) third layer.

A key feature of these samples is their asymmetric cross-section. To provide some spatial resolution to the data, a very thin diamond saw with a circular blade about 0.3 mm thick was used to section the discs into four layers as depicted schematically in Fig. 3.

Particle size distribution measurements with both the green bodies and the sintered samples likely included an error caused by either adhering or bonded grains. Both the consolidation and the bonding in the sample necessitated a redispersion of the individual grains to assess their evolution through the process. A mortar and pestle pre-treatment was made and then high ultrasonic agitation was used during the particle size distribution measurements to attempt to reduce the powder samples to a state representing the individual grains.

## 4. Results and discussion

### 4.1. Sample analysis and simulation inputs

The alumina samples were prepared as described previously. The sectioned pieces from the green body were analyzed to provide data which served as initial conditions for the simulation. To obtain this, particle size distributions from the different vertical positions were superimposed on the calculational grid by a bilinear interpolation to go from a set of four values to a  $10 \times 34$  array corresponding to the finite element grid. The area of the distributions had to be normalized in proportion to respective sample volumes. In a like-wise manner, the porosity data for the different vertical positions were interpolated in one dimension for the numerical simulation.

### 4.2. Measured results and model predictions

Fig. 4 shows the particle size distributions from the measurements taken on the powder from the structures at the different of points along the sintering path. Ostwald ripening is evident from the flattening and broadening of the curves, showing that finer particles are consumed into coarser ones. The thinner curves in this same figure show the simulated data. The forms and trends indicated match fairly well, in support of the models incorporated into the simulation which account for the sintering mechanisms. The experimental data show a weaker peak and broader distribution compared with the simulation output. Comparatively advanced coalescence between coarse and fine particles could have prevented the grinding and ultrasonic treatment from completely redispersing the grains, thereby leading to this discrepancy. Some micrographs shown in Fig. 5 demonstrate some of the above discussion. In Fig. 5a, a fracture surface from the top layer is shown. The particles are comparatively fine and well sintered. Fig. 5b shows a fracture surface from the third cut layer, where the extent of sintering is seen to be less, and the average grain sizes are larger, corresponding to their particle size distributions in Fig. 4.

The sample sections from the different sintering stages were also tested by porosimetry. These measurements are shown in Fig. 6. The pore size distributions evolve under sintering in a manner analogous to the particle size distributions. In general, as the sintering advances, the mean pore sizes become smaller and the areas under the curves also decrease, which is indicative of sample densification. The range of bulk porosities measured ranged from 46.7% at the top of the samples taken at the end of the sintering program, to 67.5% for the bottom sections of the green bodies. For each section, the curves in Fig. 6 show the same qualitative trends as curves showing the pore size distribution evolution under

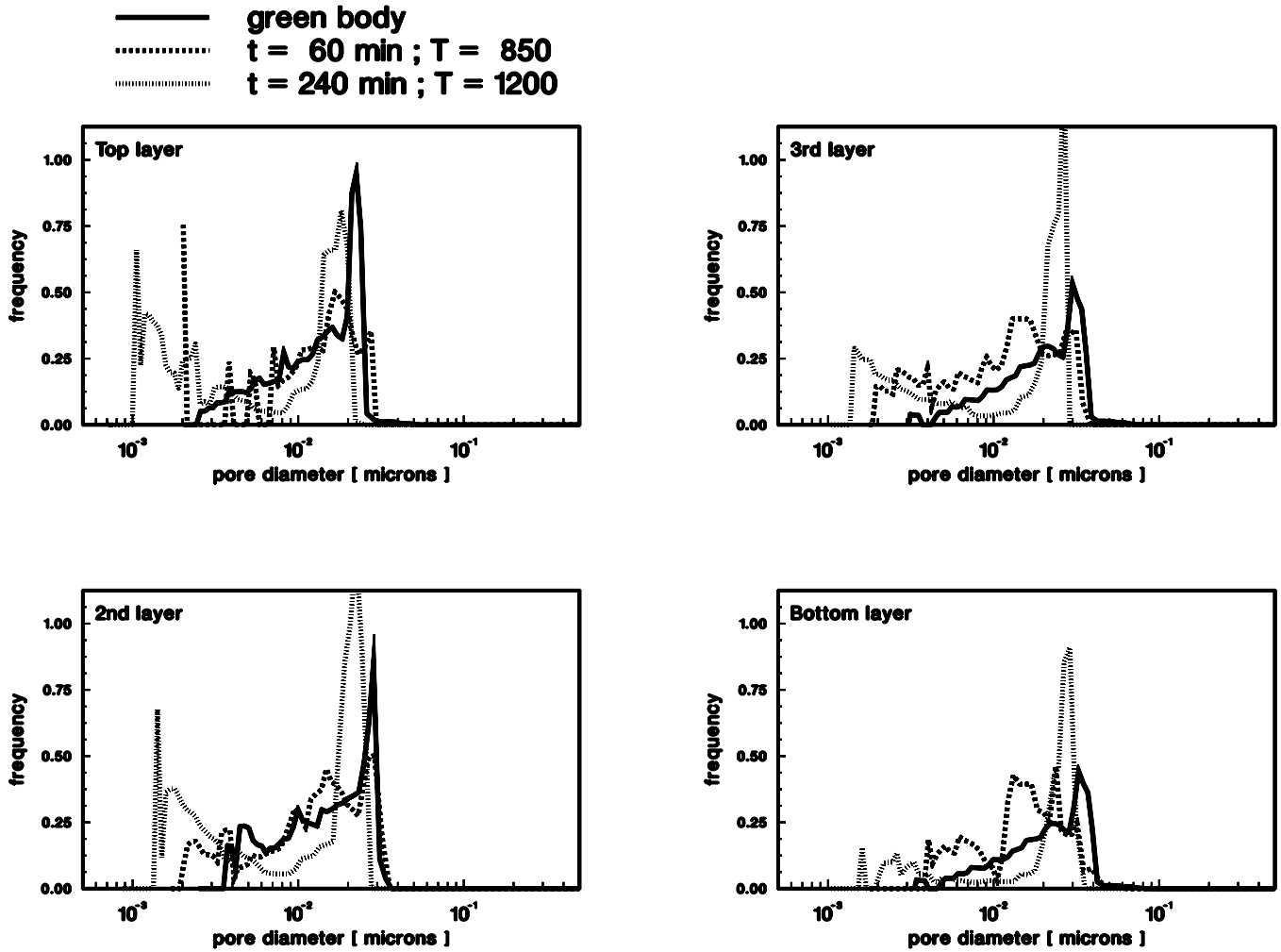


Fig. 6. Porosimetric data showing pore size distribution evolution in the samples.

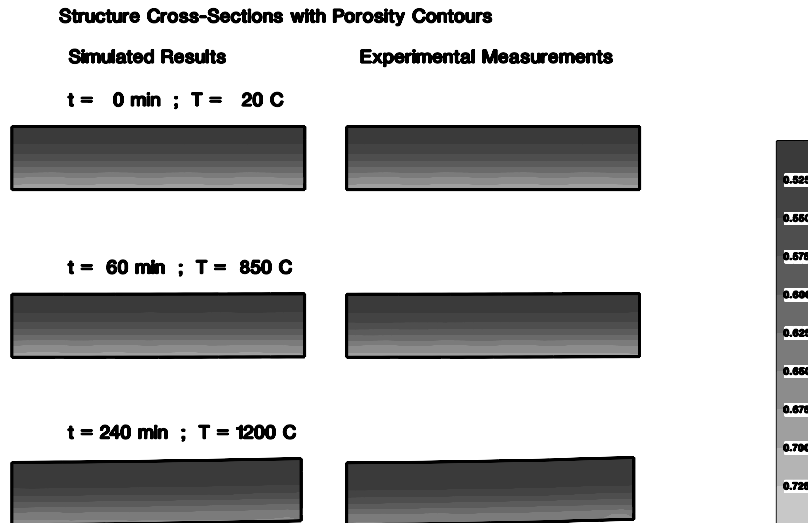


Fig. 7. Sample shape evolution over the sintering period showing density contours. Simulated results are on the left. Experimental measurements are on the right.

sintering for lithium fluoride samples [17]. The mean pore diameters increase as the point of reference is moved from top to bottom in the sample.

The effect of the saw cuts on the measurements could be considered negligible, in the sense that only the surface of the sample would be affected, while the

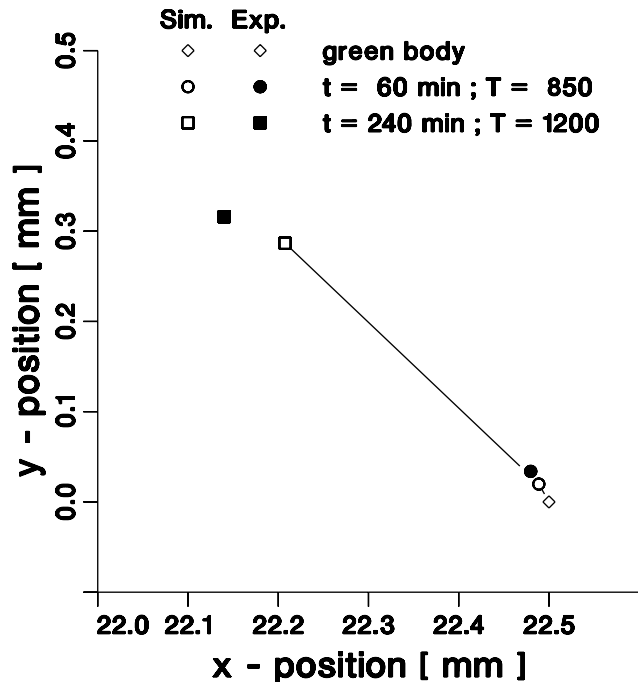


Fig. 8. Displacement vs. time for the bottom right point of the structure.

measurements of pore and grain size distribution were for bulk properties. Previous work which measured pore size distributions in horizontally sectioned top and bottom layers of a sample, as well as the overall structure, confirmed this claim [1].

#### 4.3. Shrinkage, densification and deformation

Structural information was traced by the simulation. Fig. 7 shows cross-sections of the structure at advancing times over the sintering profile, along with density contours. In general the correspondence is good. This suggests that the grain boundary diffusion sintering mechanism is the principal agent for structural evolution under the conditions imposed in this case.

Specifically, the displacement of the bottom right point of the structure is plotted in Fig. 8 for the theoretical and simulated cases. At the end of the sintering a displacement of 1.6% in the radial direction and 4.4% in the horizontal direction was observed in the sample, compared with respective values of 1.3 and 3.9% by simulation. Note that the displacement was about three times as great in the horizontal direction, indicative of the finer grain sizes along this axis compared with the plane along the bottom of the structure. This uneven shrinkage causes a small warpage in the structure, but at levels of only a few percent (in real dimensions, around 0.3 mm), the deviation from being a perfectly flat piece is acceptable for practical use. The good qualitative and quantitative correspondence between these values in-

dicated that a sufficient and suitable amount of mechanistic behavior is incorporated into the sintering model to enable it to properly trace structural evolutions of porous ceramics made from broad powder size distributions.

The present results can be further discussed in the context of related work available in the literature. A sintering simulation based on a similar constitutive model was presented by Moritz et al. [18]. In this case, the functionally gradient character was modeled as a four layer laminate, no particle size distribution effects were considered and the simulation proceeded to much higher theoretical densities, as the aim of the work was more focussed on sample warpage.

A paper by Subbanna et al. [19] provides a functional mathematical model incorporating pore shrinkage and grain growth in systems densifying under sintering. In this case, no physical mechanism is ascribed, thus exponential parameters in the model must be allowed to float to match other published data. The present simulation is a has a more direct application to real systems because its parameters are derived from experimental work, and were used in tracking the evolution of grain growth and density within the confines of a physically defined porous structure.

## 5. Conclusions

Upon formulation and numerical implementation of a model designed to demonstrate the effects of local particle size distribution effects in a porous asymmetric ceramic structure, it can be said that these effects account for observed sintering behavior in real and substantial ways. The calculated predictions corresponded well to the results obtained when physical samples with such characteristics were sintered. The presence of fines throughout the compact produced a sintered piece which bonded at lower temperatures and with less warpage. Accounting for the particle size distribution as a field variable helps to more realistically simulate the sintering results of functionally gradient materials prepared by colloiddally metastable sedimentation. For future work, this simulation tool will prove valuable in understanding microstructural effects on sintering behavior, and ultimately can aid in fabrication parameter optimization.

## References

- [1] K. Darcovich, C.R. Cloutier, Processing of functionally gradient ceramic membrane substrates for enhanced porosity, *J. Am. Ceram. Soc.* 82 (8) (1999) 2073–2079.
- [2] K. Darcovich, M.E. Price, Preparation of functionally gradient ceramic membrane substrates, *J. Can. Ceram. Soc.* 66 (2) (1997) 146–151.

- [3] K. Darcovich, M.E. Price, Microstructure processing for asymmetric ceramic membrane substrates, in: A.G. Fane (Ed.), Proceedings of the International Membrane Science and Technology Conference–IMSTEC'96, Sydney, Australia, November 12–14, 1996, pp. 164–166.
- [4] J. Cesarano, III, I.A. Aksay, A. Bleier, Stability of aqueous  $\alpha$ - $\text{Al}_2\text{O}_3$  suspensions with poly(methacrylic acid) polyelectrolyte, *J. Am. Ceram. Soc.* 71 (4) (1988) 250–255.
- [5] I.A. Aksay, Microstructure control through colloidal consolidation, in: J.A. Manjels, G.L. Messing (Eds.), *Advances in Ceramics*, vol. 9, American Ceramic Society, Columbus, OH, 1984, pp. 94–104.
- [6] A.G. Lamas, M. Almeida, H.M.M. Diz, Slip-casting of alumina bodies with differential porosities”, *Ceram. Int.* 19 (1993) 121–124.
- [7] K. Shinagawa, Finite element simulation of sintering process, *JSME Int. J. Ser. A* 39 (4) (1996) 565–572.
- [8] K. Shinagawa, Micromechanical modeling of viscous sintering and a constitutive equation with sintering stress, *Comp. Mater. Sci.* 13 (1999) 276–285.
- [9] K. Darcovich, L. Béra, K. Shinagawa, Particle size distribution effects in an FEM Model of sintering porous ceramics, *Mater. Sci. Eng. A* 341 (1–2) (2002) 247–255.
- [10] K. Shinagawa, Y. Hirashima, A constitutive model for sintering of ceramic powder compacts with internal structure due to granules, *JSME Int. J. Ser. A* 42 (1) (1999) 17–24.
- [11] R.L. Coble, A model for boundary diffusion controlled creep in polycrystalline materials, *J. Appl. Phys.* 34 (6) (1963) 1679–1682.
- [12] S. Sivakumar, P.C. Pradip, Kapur, S.G. Malghan, A size interval-by-size interval marching algorithm for modeling grain growth in the intermediate stage of sintering, *Colloids Surf. A: Physiochem. Eng. Aspects* 133 (1998) 173–182.
- [13] G.W. Greenwood, Particle coarsening, in: *The Mechanism of Phase Transformations in Crystalline Solids*, Institute of Metals, Monograph and Report Series No. 33, 1969, pp. 103–110.
- [14] J. Pan, H. Le, S. Kuchernko, J.A. Yeomans, A model for the sintering of spherical particles of different sizes by solid state diffusion, *Acta Mater.* 46 (13) (1998) 4671–4690.
- [15] M. Miyayama, K. Koumoto, H. Yanagida, Engineering properties of single oxides, in: S.J. Schneider, Jr (Ed.), *Engineered Materials Handbook*, vol. 4, ASM International, 1991, pp. 748–757.
- [16] T. Nishijima, T. Kawada, A. Ishihata, Thermal conductivity of sintered  $\text{UO}_2$  and  $\text{Al}_2\text{O}_3$  at high temperatures, *J. Am. Ceram. Soc.* 48 (1965) 31–34.
- [17] J.W. Bullard, A.W. Searcy, Microstructural development during sintering of lithium fluoride, *J. Am. Ceram. Soc.* 80 (9) (1997) 2395–2400.
- [18] T. Moritz, H. Riedel, G. Werner, G. Tomandl, Simulation and investigation of pore size graded titania layers during sintering, *J. Mater. Sci.* 35 (2000) 2235–2240.
- [19] M. Subbanna, P.C. Kapur, Pradip, Computer-aided control of the evolution of microstructure during sintering, *Mater. Chem. Phys.* 67 (2001) 17–24.